An examination of complex fractional order physical phenomena in IOPD controller design

An examination of complex fractional order physical phenomena in IOPD controller design

Uğur Demiroglu[1], Bilal Şenol[2], Radek Matušů[3]

[1]*Computer Sciences Department, Technical Vocational School, Firat University, Elazig, Turkiye*

[2]*Software Engineering Department, Faculty of Engineering, Aksaray University, Aksaray, Turkiye*

[3]*Centre for Security, Information and Advanced Technologies (CEBIA-Tech), Faculty of Applied Informatics, Tomas Bata University in Zlín, Zlin, Czech Republic*

Correspondence Uggur: Demirogglu, Computer Sciences Department, Technical Vocational School, Firat University, Elazigg, Turkiye. Email: ugurdemiroglu@firat.edu.tr

This research focuses on the fractional complex order plant ($FCOP$). The significant contribution is the role of complex plant models in system stability and robustness and associated physical phenomena. A general transfer function is studied in the paper. Other plant models may be built with this structure since the $FCOP$ is a general mathematical form covering integer order plant (IOP) and fractional order plant (FOP). Using the equations produced with the proposed technique and the recommended integer order proportional derivative ($IOPD$ controller, physical changes in integer, fractional and complex coefficients, and orders are observed within this paper. Analysis of the plant controlled with an $IOPD$ controller is done by applying an integrator to reveal the differences. The effects of the parameters are discussed together with the visuals, supported by simulations. The aim is to tune the controller parameters to achieve the phase and specifications as the researcher desired. It is observed that the integrator greatly takes part in reducing the steady-state error. The IOP with the integrator showed the lowest steady-state error, and also, the settling and overshoot time were enhanced. Increase in the phase margin also caused an increase in the phase crossover frequency. It is also observed that the fractional order affected the phase crossover frequency comparing with the IOP, and the complex order modification also had an effect comparing to the fractional order version. The complex order of the system is considered with its conjugate components in the imaginary part thus, the results are found separately for each case.

KEYWORDS: Analytical method, controller design, fractional complex order, fractional order, integer order, proportional derivative

1 INTRODUCTION

The Proportional-Integral-Derivative (PID) control is a general and efficient solution to real-world control issues because of its three-term functionality, which treats both transient and steady-state responses [**1**]. The three main control effects seen in current controllers are investigated, and practical

names and units of measurement for each impact are provided [**2**]. Because of its sturdy performance and simplicity, PID controllers are widely employed in the process industries. Indeed, more than 90% of control loops are of PID, while the majority of loops are PI since derivative action is rarely utilized [**3, 4**]. By adding non-integer derivative and integral elements in the plant model or controller, fractional calculus allows greater degrees of freedom in modeling and control of dynamical systems [**5-7**]. Given the fact that complex order differentiation was formally described many years ago, complex order transfer functions are not as commonly employed as real order ones. In comparison to real-order controllers, fractional complex order controllers contain more parameters. As a result, a greater number of objectives can be met [**8, 9**]. With the work of Liouville and Riemann at the turn of the nineteenth century, the generalization of differentiation to real or complex orders was formalized [**10, 11**]. Afterwards, number of the related studies had a sharp increase. For example, Abdulwahhab et al. obtained both real and complex fractional order PID controllers that are constructed for a low pressure flowing water circuit, which is a First Order Plus Time Delay system [**12**]. The focus of Bingi et al. was to create a sophisticated fractional order differentiator and integrator for the order $\alpha + j\beta$ in a previous study [**13**]. Stability region design of fractional complex order PI controller using D segmentation is the topic of Zheng et al. in a previous study [**14**]. Tuning of complex coefficient $PI/PD/PID$ controllers for a universal plant structure is the emphasis of Sathishkumar et al. in a previous study [**15**]. Sathishkumar et al.'s structure was for integer/fractional order plants with real coefficient and dead time in a previous study [**16**]. In order to guarantee system robustness against gain and noise, Guefrachi et al. in a previous study [**8**] suggested a novel fractional complex order control structure management based on an optimization design. Hanif et al. used the genetic algorithm to improve the performance of the new form of fractional complex order controller in a previous study [**17**]. Sekhar et al. used the complex order PID for surface roughness control in machining of $CNT\ Al - Mg$ hybrid composites in a previous study [**18**]. Saikumar et al. described the development of a complex order filter and its subsequent integration into a PID-based controller design in a previous study [**19**]. Due to the relation with fractional order differentiation, the studies on the problems related to partial differential equations should be useful to cite too. For example, a $(2+1)$ and a $(3+1)$-dimensional sine-Gordon equation and a sinh-Gordon equation are derived in the studies [**20, 21**], and a new $(3+1)$-dimensional Schrodinger equation in Quantum Mechanics is derived by Wang [**22**]. It would also be useful to give brief information about the Lie group studies. A group that is also a differentiable manifold is called a Lie group. Groups define the abstract concept of a binary operation along with the additional properties it must have to be thought of as a "transformation" in the abstract sense, such as multiplication and the taking of inverses or, alternatively, the concept of addition and the taking of inverses. A manifold is a space that locally resembles Euclidean space. Combining these two concepts results in a continuous group with continuous multiplying points and inverses. A Lie group can be obtained if the multiplication and taking of inverses are both smooth. In this direction, a systematic study of the generalized KdV-Burgers-Kuramoto equation using the symmetry method is presented in a previous study [**23**], a new $(3+1)$-dimensional KdV equation and MKdV equation with their corresponding fractional forms are presented in another study [**24**], and the modified Gardner type equation and its time fractional form is studied by Wang and Wazwaz [**25**]. Researchers are now investigating the use of complex order differ-integral operators in control theory and system modeling [**26-36**]. Although not exactly the same as this paper, there can be found studies in the literature aiming to provide frequency specifications. The common aim of these studies is to tune a convenient controller to achieve robustness against gain changes; hence, in this paper, a different point of view is utilized [**37, 38**]. When the approach in this paper is compared with the previous studies, the goal of tuning the controller parameters to obtain desired phase specifications is in a similar way. However, these studies brought mathematical complications when providing the robustness by setting the phase

derivative to zero at the phase crossover frequency [**39-41**]. The approach in this paper is totally an analytical point of view.

Using the $FCOP$ model and integer order proportional derivative ($IOPD$) controller structure, which are becoming more and more widespread in applied physics and control systems, the goal of this work is to generate analytical solutions and evaluate the physical phenomena of these results. The classical proportional derivative controller structure with a complex system is considered, which has received little attention in the literature so far. The results of the solutions for the stability and robustness of the system achieved with various values of the parameters are discussed and supported by simulations and visuals. The effects of the real and imaginary components of the complex number in the process are observed from a different point of view in system design.

2 SPECIFICATIONS FOR A CLOSED LOOP CONTROL SYSTÉM

Figure 1 depicts the closed loop control system block diagram employed in this study.

The input Laplace sign of the system is R(s), and the output Laplace sign is Y(s). P(s) denotes the controlled system, and C(s) is the controller. The system's open loop transfer function is now known as G(s) and may be found in Equation (**1**).

$$R(s)C(s)P(s) = Y(s) \Rightarrow G(s) = \frac{Y(s)}{R(s)} = C(s)P(s) \tag{1}$$

T(s) is the closed-loop transfer function of the system, which may be found in Equation (**2**).

$$(R(s) - Y(s))C(s)P(s) = Y(s) \Rightarrow T(s) = \frac{Y(s)}{R(s)} = \frac{C(s)P(s)}{1 + C(s)P(s)} = \frac{G(s)}{1 + G(s)} \tag{2}$$

As can be observed, the system's closed-loop transfer function is closely related to its open-loop transfer function.

3 SPECIFICATIONS FOR AN OPEN LOOP CONTROL SYSTEM

The Bode diagram is a graph that shows the system's gain and phase margin curves together. Illustrating two system components in a single image at the same time is quite convenient. In the analysis of open loop systems, Bode diagrams are utilized. In the diagram, the gain crossover frequency is ω_{gc} and the phase crossover frequency is ω_{pc}. The gain crossover frequency is the frequency at which the gain curve cuts OdB. Similarly, the frequency value where the phase curve cuts -180° is known as phase crossover frequency. The gain margin (GM) shows how much the open loop system's gain can be increased before reaching system instability. Similarly, the phase margin (PM) specifies how much the open loop system's phase can be increased before reaching system instability [**37, 42, 43**].

Equations (**3**)-(**4**) give the phase and gain of the system at the gain crossover frequency, and Equations (**5**)-(**6**) give the phase and gain of the system at the phase crossover frequency. These specifications will be used throughout the paper.

$$\angle G(s)|_{s=j\omega_{gc}} = PM - \pi \tag{3}$$

$$|G(s)||_{s=j\omega_{gc}} = 1 \tag{4}$$

$$\angle G(s)|_{s=j\omega_{pc}} = -\pi \tag{5}$$

$$|G(s)||_{s=j\omega_{pc}} = 10^{GM/20} \tag{6}$$

As can be told from the above equations, the gain and phase crossover frequencies in the Bode diagram are closely related to the system's stability and robustness across a large range.

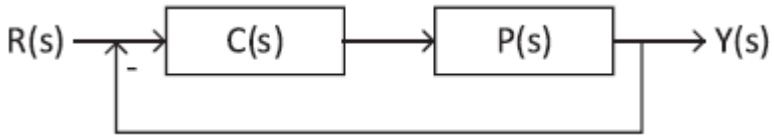

FIGURE 1 Block schematic of a closed loop control system.

4 DISTURBANCE IN THE LOAD

The current error of a system increases when it encounters unexpected load disturbance signals. Unwanted external input signal to the system is what this circumstance is defined as. In control studies, design of a stable system is important. In stable systems, avoiding or fully eliminating system failures that may emerge as a result of such unexpected load disturbance signals makes the design process even more critical. **Figure 2** depicts the system load disturbance block diagram used in this study [**44-46**].

The unit step signal is described in **Figure 3** as an unexpected load disturbance signal at any time when the system is in the steady state. In this study, a certain value will be used as the time value after the step response of the system has settled.

Equation (**7**) gives the partial function representation of the load disturbance signal.

$$u(t-a)=\begin{cases}1 & t\geq a\\ 0 & t<a\end{cases} \tag{7}$$

The charge disturbance signal's D(s) input Laplace sign is obtained in Equation (**8**) by converting $d(t) = u(t - a)$.

$$D(s)=\frac{1}{s}\mathrm{e}^{-as} \tag{8}$$

In the findings of the development of the systems utilized in this study, $MATLAB$, the multi-paradigm numerical computing software, was used to display the response of the system under load disturbance. Simulink, a $MATLAB$-based graphical programming environment, has been used to model, simulate, and evaluate dynamic systems. **Figure 4** shows the Simulink circuit diagram for the system under load disturbance.

The results of this study were achieved using a computer with an Intel® Core™ i5-4460 CPU running at 3.20 GHz, RAM of 12.0 GB, and a 64-bit operating system with an ×64-based processor.

5 DESIGN OF THE UNIVERSAL PLANT

Equation (9) is a general representation of a plant transfer function that can include integer, fractional, and complex number coefficients or orders, time-delayed, or non-delayed extra gain coefficients.

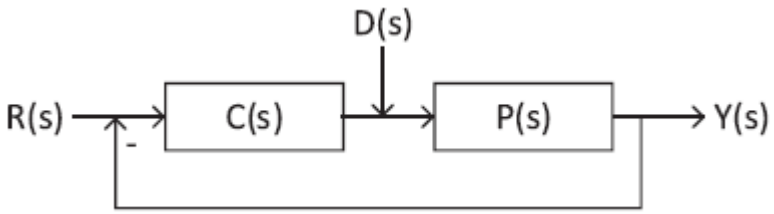

FIGURE 2 Block schematic of system load disturbance.

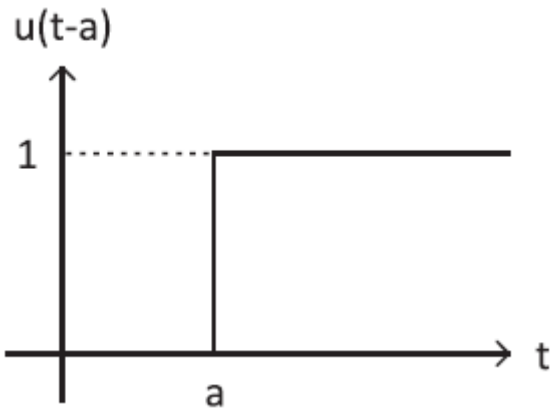

FIGURE 3 Load disturbance signal.

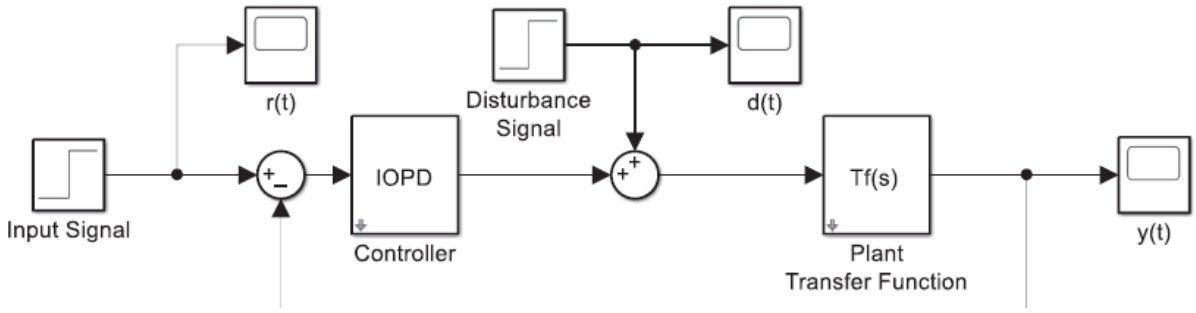

FIGURE 4 Simulink circuit schematic for a system with a load disturbance.

Here, the gain is K, and the time delay coefficient is L. The i^{th} even part of the complex coefficients of the numerator polynomial is represented by a_{ei}, whereas the i^{th} odd part is represented by ao_i. In the similar way, be_k represents the k^{th} even part of the complex coefficients of the denominator polynomial and bo_k represents the k^{th} odd part.

Likewise, the i^{th} even part of the complex orders of the numerator polynomial is represented by ae_i and the ith odd component is represented by ao_i. βe_k represents the k^{th} even part of the complex orders of the denominator polynomial, and βo_k represents the k^{th} odd part.

Equation (**10**) gives the frequency response representation of the above plant.

$$P(j\omega) = K\frac{\sum_{i=0}^{m}(j\omega)^{\alpha e_i + j\alpha o_i}(ae_i + jao_i)}{\sum_{k=0}^{n}(j\omega)^{\beta e_k + j\beta o_k}(be_k + jbo_k)}e^{-L(j\omega)} \tag{10}$$

With the use of Euler's equation, a complex number can be transformed from its trigonometric form to its exponential and also from its exponential form to its trigonometric form. In this direction, Equation (**11**) shows the trigonometric expression of a complex order ($j\omega$) in the numerator polynomial.

$$(j\omega)^{\alpha e_i+j\alpha o_i} = e^{-\frac{\pi\alpha o_i}{2}}\omega^{\alpha e_i}\left(\cos\left(\frac{\pi\alpha e_i}{2}+\log(\omega)\alpha o_i\right)+j\sin\left(\frac{\pi\alpha e_i}{2}+\log(\omega)\alpha o_i\right)\right) \tag{11}$$

Similarly, Equation (**12**) stands for the trigonometric expression of a complex order ($j\omega$) in the denominator polynomial.

$$(j\omega)^{\beta e_k+j\beta o_k} = \mathrm{e}^{-\frac{\pi\beta o_k}{2}}\omega^{\beta e_k}\left(\cos\left(\frac{\pi\beta e_k}{2}+\log(\omega)\beta o_k\right)+j\sin\left(\frac{\pi\beta e_k}{2}+\log(\omega)\beta o_k\right)\right) \tag{12}$$

Then, the plant frequency response can be re-expressed as in Equation (**13**) by changing the formulas in Equations (**11**) and (**12**) to exponential form.

$$P(j\omega) = K\frac{\sum_{i=0}^{m}\mathrm{e}^{-\frac{\pi\alpha o_i}{2}}\omega^{\alpha e_i}\mathrm{e}^{j\left(\frac{\pi\alpha e_i}{2}+\log(\omega)\alpha o_i\right)}(ae_i+jao_i)}{\sum_{k=0}^{n}\mathrm{e}^{-\frac{\pi\beta o_k}{2}}\omega^{\beta e_k}\mathrm{e}^{j\left(\frac{\pi\beta e_k}{2}+\log(\omega)\beta o_k\right)}(be_k+jbo_k)}\mathrm{e}^{-jL\omega} \tag{13}$$

Equation (**14**) re-expresses the plant frequency response described in Equation (**13**) in a more simple form.

$$P(j\omega) = K\frac{(ne+jno)}{(de+jdo)}\mathrm{e}^{-jL\omega} \tag{14}$$

Here, ne and no stand for the even and odd parts of the numerator polynomial, respectively. Similarly, de and do are the even and odd parts of the denominator polynomial, respectively. Equations (**15**)-(**16**) show the frequency response representations of ne and no, respectively.

$$ne = \sum_{i=0}^{m}\mathrm{e}^{-\frac{\pi\alpha o_i}{2}}\omega^{\alpha e_i}\left(\cos\left(\frac{\pi\alpha e_i}{2}+\log(\omega)\alpha o_i\right)ae_i-\sin\left(\frac{\pi\alpha e_i}{2}+\log(\omega)\alpha o_i\right)ao_i\right) \tag{15}$$

$$no = \sum_{i=0}^{m}\mathrm{e}^{-\frac{\pi\alpha o_i}{2}}\omega^{\alpha e_i}\left(\sin\left(\frac{\pi\alpha e_i}{2}+\log(\omega)\alpha o_i\right)ae_i+\cos\left(\frac{\pi\alpha e_i}{2}+\log(\omega)\alpha o_i\right)ao_i\right) \tag{16}$$

Equations (**17**)-(**18**) show the frequency response representations of de and do, respectively.

$$de = \sum_{k=0}^{n}\mathrm{e}^{-\frac{\pi\beta o_k}{2}}\omega^{\beta e_k}\left(\cos\left(\frac{\pi\beta e_k}{2}+\log(\omega)\beta o_k\right)be_k-\sin\left(\frac{\pi\beta e_k}{2}+\log(\omega)\beta o_k\right)bo_k\right) \tag{17}$$

$$do=\sum_{k=0}^{n} e^{-\frac{\pi\beta o_k}{2}}\omega^{\beta e_k}\left(\sin\left(\frac{\pi\beta e_k}{2}+\log(\omega)\beta o_k\right)be_k+\cos\left(\frac{\pi\beta e_k}{2}+\log(\omega)\beta o_k\right)bo_k\right) \tag{18}$$

Using complex number theory, the frequency response representation can be summarized in its gain and phase parts as

$$P(j\omega)=|P(j\omega)|e^{j\angle \mathrm{P}(j\omega)}. \tag{19}$$

Referring to the above equation, Equation (**20**) gives the gain value of the plant frequency response.

$$|P(j\omega)|=K\sqrt{\frac{ne^2+no^2}{de^2+do^2}} \tag{20}$$

Likewise, Equation (**21**) gives the phase value of the plant frequency response.

$$\angle \mathrm{P}(j\omega)=\arctan\left(\frac{no}{ne}\right)-\arctan\left(\frac{do}{de}\right)-L\omega \tag{21}$$

As a consequence for this section, the gain and phase equations for the plant frequency response were found.

6 DESIGN OF THE UNIVERSAL PLANT WITH AN INTEGRATOR

Equation (**22**) is the plant transfer function with an integrator produced by multiplying the transfer function given in Equation (**9**) by 1/s. The components of the plant with the integrator will be shown with a^* from this point forward.

$$P(s)^*=\frac{1}{s}P(s)=K\frac{\sum_{i=0}^{m}(ae_i+jao_i)s^{(\alpha e_i+j\alpha o_i)}}{\sum_{k=0}^{n}(be_k+jbo_k)s^{(1+\beta e_k+j\beta o_k)}}e^{-Ls} \tag{22}$$

Equation (**23**) shows the frequency response of plant with the integrator in Equation (**22**).

$$P(j\omega)^*=K\frac{\sum_{i=0}^{m}(j\omega)^{\alpha e_i+j\alpha o_i}(ae_i+jao_i)}{\sum_{k=0}^{n}(j\omega)^{1+\beta e_k+j\beta o_k}(be_k+jbo_k)}e^{-L(j\omega)} \tag{23}$$

As the integrator affects the denominator polynomial, trigonometric transformation of the complex order operator of the denominator is given below.

$$(j\omega)^{1+\beta e_k+j\beta o_k}=\mathrm{e}^{-\frac{\pi\beta o_k}{2}}\omega^{1+\beta e_k}\left[\cos\left(\frac{\pi(1+\beta e_k)}{2}+\log(\omega)\beta o_k\right)+j\sin\left(\frac{\pi(1+\beta e_k)}{2}+\log(\omega)\beta o_k\right)\right] \tag{24}$$

The frequency response of the plant with integrator can be re-expressed as given in Equation (**25**) by converting the formulas in Equations (**11**) and (**24**)to the exponential form.

$$P(j\omega)^*=K\frac{\sum_{i=0}^{m}\mathrm{e}^{-\frac{\pi\alpha o_i}{2}}\omega^{\alpha e_i}\mathrm{e}^{j\left(\frac{\pi\alpha e_i}{2}+\log(\omega)\alpha o_i\right)}(ae_i+jao_i)}{\sum_{k=0}^{n}\mathrm{e}^{-\frac{\pi\beta o_k}{2}}\omega^{1+\beta e_k}\mathrm{e}^{j\left(\frac{\pi(1+\beta e_k)}{2}+\log(\omega)\beta o_k\right)}(be_k+jbo_k)}\mathrm{e}^{-jL\omega} \tag{25}$$

Simplified representation of the above equation is given in Equation (**26**).

$$P(j\omega)^*=K\frac{(ne+jno)}{(de^*+jdo^*)}\mathrm{e}^{-jL\omega} \tag{26}$$

Here, the even and odd parts of the numerator polynomial are the same as given previously. In Equations (**27**)-(**28**), the frequency response of de^* (even part) and do^* (odd part) of the denominator polynomial of the system with the integrator are given respectively.

$$de^*=\sum_{k=0}^{n}\mathrm{e}^{-\frac{\pi\beta o_k}{2}}\omega^{1+\beta e_k}\begin{bmatrix}-\sin\left(\frac{\pi\beta e_k}{2}+\log(\omega)\beta o_k\right)be_k\\-\cos\left(\frac{\pi\beta e_k}{2}+\log(\omega)\beta o_k\right)bo_k\end{bmatrix} \tag{27}$$

$$do^*=\sum_{k=0}^{n}\mathrm{e}^{-\frac{\pi\beta o_k}{2}}\omega^{1+\beta e_k}\left[\cos\left(\frac{\pi\beta e_k}{2}+\log(\omega)\beta o_k\right)be_k-\sin\left(\frac{\pi\beta e_k}{2}+\log(\omega)\beta o_k\right)bo_k\right] \tag{28}$$

As the result, Equation (**29**) gives the gain of the plant's frequency response with integrator and Equation (**30**) gives the phase of the plant's frequency response with integrator.

$$|P(j\omega)^*|=K\sqrt{\frac{ne^2+no^2}{(de^*)^2+(do^*)^2}} \tag{29}$$

$$\angle\mathrm{P}(j\omega)^*=\arctan\left(\frac{no}{ne}\right)-\arctan\left(\frac{do^*}{de^*}\right)-L\omega \tag{30}$$

7 DESIGN OF THE PD CONTROLLER

The classical $IOPD$ controller's transfer function is described in Equation (**31**).

$$C(s) = k_p + k_d s \tag{31}$$

The proportional coefficient of the controller is indicated by k_p. Likewise, k_d shows the derivative coefficient. Equation (**32**) shows the frequency response of the $IOPD$ controller.

$$C(j\omega) = k_p + jk_d\omega \tag{32}$$

The frequency response of the $IOPD$ controller showing its gain and phase parts is given in Equation (**33**).

$$C(j\omega) = |C(j\omega)|e^{j\angle C(j\omega)} \tag{33}$$

From the above equation, gain and phase of the controller frequency response are given in Equations (**34**) and (**35**), respectively.

$$|C(j\omega)| = \sqrt{k_p^2 + k_d^2\omega^2} \tag{34}$$

$$\angle C(j\omega) = \arctan\left(\frac{k_d\omega}{k_p}\right) \tag{35}$$

Thus, the frequency response of the controller is found.

8 DESIGN OF THE AUTO TUNING SYSTÉM

Equation (**36**) gives the frequency response of the system of the plant and the controller.

$$G(j\omega) = C(j\omega)P(j\omega) \tag{36}$$

Then, gain and phase of the system can be found using the representaions in Equations (**37**)-(**38**).

$$|G(j\omega)| = |C(j\omega)P(j\omega)| = |C(j\omega)||P(j\omega)| \tag{37}$$

$$\angle \mathrm{G}(j\omega) = \angle \mathrm{C}(j\omega)\mathrm{P}(j\omega) = \angle \mathrm{C}(j\omega) + \angle \mathrm{P}(j\omega) \tag{38}$$

Notations in Equation (**39**) will be used in future expressions to make a convenience in the calculation of system gain and phase at the gain crossover frequency ω_{gc}.

$$\begin{aligned} gcne &= ne|_{\omega=\omega_{gc}} \quad gcno = no|_{\omega=\omega_{gc}} \\ gcde &= de|_{\omega=\omega_{gc}} \quad gcdo = do|_{\omega=\omega_{gc}} \end{aligned} \tag{39}$$

From Equation (**37**), gain of the system at the gain crossover frequency is given in Equation (**40**).

$$\begin{aligned} |G(j\omega_{gc})| &= |C(j\omega_{gc})||P(j\omega_{gc})| \\ &= \sqrt{k_p^2 + k_d^2\omega_{gc}^2}K\sqrt{\frac{gcne^2 + gcno^2}{gcde^2 + gcdo^2}} = 1 \end{aligned} \tag{40}$$

Similarly, from Equation (**38**), phase of the system at ω_{gc} is given in Equation (**41**).

$$\begin{aligned} \angle \mathrm{G}(\mathrm{j}\omega_{gc}) &= \angle \mathrm{P}(\mathrm{j}\omega_{gc}) + \angle \mathrm{C}(\mathrm{j}\omega_{gc}) \\ &= \arctan\left(\frac{gcno}{gcne}\right) - \arctan\left(\frac{gcdo}{gcde}\right) - L\omega_{gc} + \arctan\left(\frac{k_d\omega_{gc}}{k_p}\right) = PM - \pi \end{aligned} \tag{41}$$

Following substitution in Equation (**41**) is done to calculate the $IOPD$ controller's performance coefficients.

$$\frac{k_d\omega_{gc}}{k_p} = \tan(\varphi_1) \tag{42}$$

Here, φ_1 is

$$\varphi_1 = PM - \pi - \arctan\left(\frac{gcno}{gcne}\right) + \arctan\left(\frac{gcdo}{gcde}\right) + L\omega_{gc}. \tag{43}$$

From above equations, k_1 and k_2 of the $IOPD$ controller are obtained for ω_{gc} and given in Equation (**44**). Here, $k_p = k_1$ and $k_d = k_1k_2$ replacing is considered in order to minimize the calculation cost.

$$k_1 = \pm \frac{\sqrt{gcde^2 + gcdo^2}}{K\sqrt{(gcne^2 + gcno^2)\sec(\varphi_1)^2}}$$
$$k_2 = \frac{\tan(\varphi_1)}{\omega_{gc}} \tag{44}$$

Now, one can find the controller parameters for the phase crossover frequency. From this point forward, notations in Equation (**45**) will be used to make a convenience in the calculation of system gain and phase at the phase crossover frequency ω_{pc}.

$$pcne = ne|_{\omega=\omega_{pc}} \quad pcno = no|_{\omega=\omega_{pc}}$$
$$pcde = de|_{\omega=\omega_{pc}} \quad pcdo = do|_{\omega=\omega_{pc}} \tag{45}$$

From the frequency specifications given previously, gain and phase of the system at the phase crossover frequency is given in Equations (**46**) and (**47**), respectively.

$$|G(j\omega_{pc})| = |P(j\omega_{pc})||C(j\omega_{pc})|$$
$$= K\sqrt{\frac{pcne^2 + pcno^2}{pcde^2 + pcdo^2}}\sqrt{k_p^2 + k_d^2\omega_{pc}^2} = 10^{GM/20} = DB \tag{46}$$

$$\angle G(j\omega_{pc}) = \angle P(j\omega_{pc}) + \angle C(j\omega_{pc})$$
$$= \arctan\left(\frac{pcno}{pcne}\right) - \arctan\left(\frac{pcdo}{pcde}\right) - L\omega_{pc} + \arctan\left(\frac{k_d\omega_{pc}}{k_p}\right) = -\pi \tag{47}$$

Again, for ω_{pc}, substitution shown in Equation (**48**) is made in Equation (**47**) to calculate the controller coefficients.

$$\frac{k_d\omega_{pc}}{k_p} = \tan(\varphi_2), \tag{48}$$

where φ_2 is

$$\varphi_2 = -\pi - \arctan\left(\frac{pcno}{pcne}\right) + \arctan\left(\frac{pcdo}{pcde}\right) + L\omega_{pc}. \tag{49}$$

Substitutions of $k_p = k_1$ and $k_d = k_1\, k_2$ are made to reduce the cost of calculation and then, k_1 and k_2 of the $IOPD$ controller are obtained for ω_{pc} and given in Equation (**50**).

$$k_1 = \pm \frac{DB\sqrt{pcde^2 + pcdo^2}}{K\sqrt{(pcne^2 + pcno^2)\sec(\varphi_2)^2}}, \quad DB = 10^{\frac{GM}{20}}$$
$$k_2 = \frac{\tan(\varphi_2)}{\omega_{pc}} \tag{50}$$

Now, the controller parameters to satisfy the frequency specifications in both crossover frequencies are obtained. The next is to combine the seperately found parameters to achieve the specifications at the same time. The DB and GM can be derived by solving the k_1's in Equations (**44**) and (**50**) together. At the same time, together, the solution of the k_2's in these equations yields the mpc phase crossover frequency, which corresponds to the mgc gain crossover frequency. In fact, in this method, the largest frequency range that the system can work with are obtained without giving an external value to the gain crossover frequency.

On both the gain and phase crossover values of the above equations of k_2, numerical analysis steps created by tracking the common intersection points of the two equations are applied to deter+mine the gain crossover frequency. As the result, specified unknowns are discovered and the k_p and k_d values are generated using the substitution approach. The replacement method is used to validate the accuracy and validity of the data produced at the previous stage.

9 I DESIGN OF THE AUTO TUNING SYSTEM WITH AN INTEGRATOR

As stated before, the components of the plant with the integrator were shown with a^* sign. Notations in Equation (**51**) will be used to make a convenience in the calculation of this system's gain and phase at the gain crossover frequency ω_{gc}.

$$gcne = ne|_{\omega=\omega_{gc}} \quad gcno = no|_{\omega=\omega_{gc}}$$
$$gcde^* = de^*|_{\omega=\omega_{gc}} \quad gcdo^* = do^*|_{\omega=\omega_{gc}} \tag{51}$$

Then, the gain of the system can be obtained in a similar way to Equation (**40**). Also, the phase of the system can be obtained as in Equation (**41**). Here, the steps are in the same order as given in Equations (**41**), (**42**), and (**43**). Again, substitutions of $k_p = k_1$ and $kd = k_1k_2$ are used to simplify the calculation. Consequently, k_1 and k_2 are obtained for ω_{gc} as given in Equation (**52**).

$$k_1 = \pm \frac{\sqrt{(gcde^*)^2 + (gcdo^*)^2}}{K\sqrt{(gcne^2 + gcno^2)\sec(\varphi_1^*)^2}}$$
$$k_2 = \frac{\tan(\varphi_1^*)}{\omega_{gc}} \tag{52}$$

Equation (**53**) shows the notations to calculate the gain and phase of the system with integrator at the phase crossover frequency.

$$\begin{aligned} pcne &= ne|_{\omega=\omega_{pc}} \quad pcno = no|_{\omega=\omega_{pc}} \\ pcde^* &= de^*|_{\omega=\omega_{pc}} \quad pcdo^* = do^*|_{\omega=\omega_{pc}} \end{aligned} \tag{53}$$

Gain and phase of the system can separately be obtained by the help of Equations (**46**) and (**47**), respectively. After applying the steps in Equations (**47**), (**48**), and (**49**), coefficients of the controller can be found. Thus, controller parameters are found for the phase crossover frequency as given in Equation (**54**).

$$\begin{aligned} k_1 &= \pm \frac{DB\sqrt{(pcde^*)^2 + (pcdo^*)^2}}{K\sqrt{(pcne^2 + pcno^2)\sec(\varphi_2^*)^2}}, \quad DB = 10^{\frac{GM}{20}} \\ k_2 &= \frac{\tan(\varphi_2^*)}{\omega_{pc}} \end{aligned} \tag{54}$$

Hence, the gain and phase calculations of the system are completed.

10 CASE STUDY

In this section, four examples including systems of integer order, fractional order, and fractional complex order are considered. Bode diagrams, step responses, and responses under unexpected load disturbances will be created for each controlled system during the stability analysis. The distinctions in plant structure changes from the most basic to the most complex under constant conditions will be shown in each application.

10.1 Example 1: Integer order plant (IOP)

Consider the plant Equation (**55**) utilized by Onat et al. in their research [**47**].

$$P_1(s) = \frac{1}{s+1}e^{-s} \tag{55}$$

The desired gain crossover frequency is ω_{gc} — 1.5rad/s, and the PM is 45° in this example. As a result, Equation (**56**) shows the controller that is generated using Equations (**44**) and (**50**).

$$C_1(s) = 1.78835 + 0.151747s \tag{56}$$

Figure 5 shows the intersection point found by the numerical analysis of k_2, and the Bode diagram of the system, with a PM of 45°. It is clear in **Figure 5** that the system meets the specified conditions with the proposed controller.

Figure 6 shows the step response of the system without and with the load disturbance. In the first part, the step response shows a behavior with a steady-state error because of the lack of the integrator. In the second part, the system keeps it stable response under unexpected load disturbance and the steady-state error is reduced to zero.

Table 1 shows the mpc, GM, k_p, and k_d values according to the PM values between 30° and 60° with the increment of 5° using the proposed equations.

It can be seen in **Table 1** that the rise in the PM value causes the ω_{pc} to increase and move away from the ω_{gc}. This result demonstrates that the PM value has a direct effect on the ω_{pc}.

Figure 7 shows the intersection points and Bode diagrams of the system obtain with the PM in the range $PM = [30°, 60°]$. $\omega_{gc}^{<1>}$ represents the system with $PM = 30°$, and $\omega_{gc}^{<7>}$ represents the system with $PM = 60°$.

Similarly, **Figure 8** shows the step responses with and without load disturbance of the system with $PM = [30°, 60°]$ degrees. The load disturbance caused about 40% increment in the steady state of the step response.

It can be concluded that the system shows stable and robust response using the equations derived with the proposed technique.

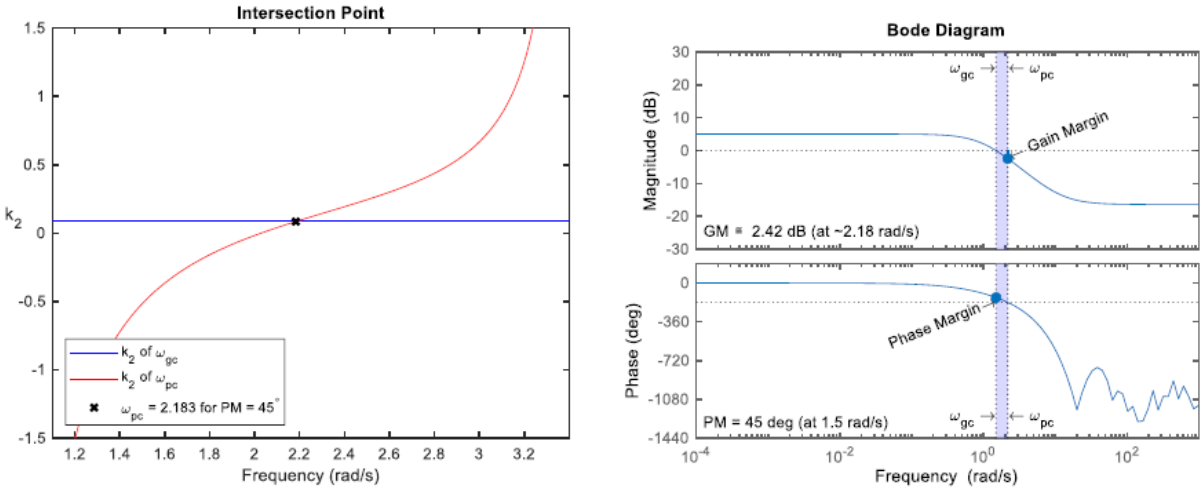

FIGURE 5 The intersection point of the k_2 values and Bode diagram with $PM = 45°$. [Colour figure can be **viewed at wileyonlinelibrary. com**]

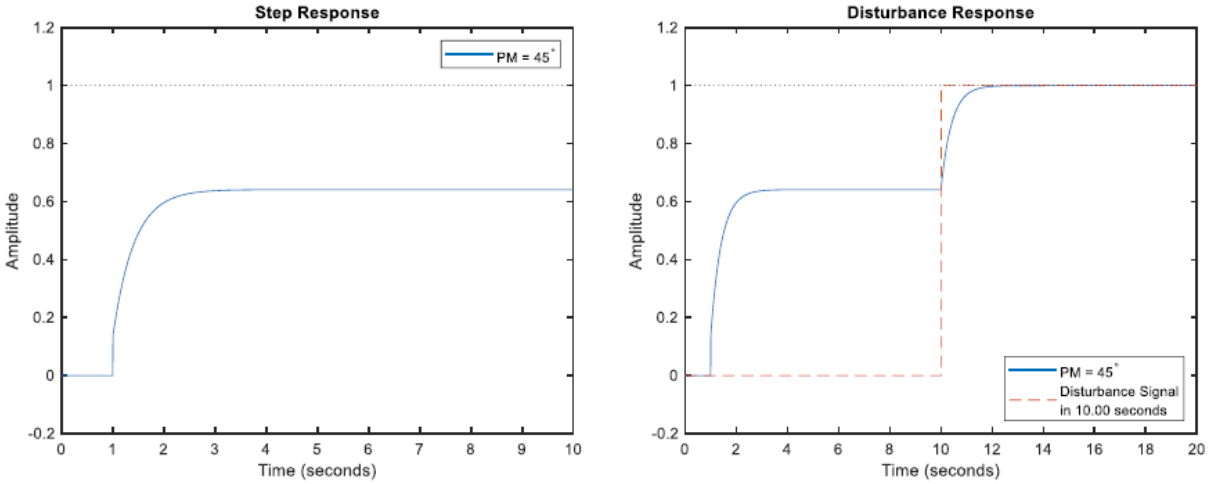

FIGURE 6 The step response of the system and its load disturbance reaction with $PM = 45°$. [Colour figure can be viewed at **wileyonlinelibrary.com**]

TABLE 1 ω_{pc}, GM, k_p, and k_d found for varying PM values.

PM	ω_{gc}	ω_{pc}	GM	k_p	k_d
30°	1.5	1.88824	−1.43013	1.78632	−0.161996
35°	1.5	1.97615	−1.78037	1.80070	−0.057587
40°	1.5	2.07437	−2.12027	1.80138	0.047260
45°	1.5	2.18347	−2.41429	1.78835	0.151747
50°	1.5	2.30233	−2.61759	1.76170	0.255080
55°	1.5	2.42729	−2.68633	1.72165	0.356471
60°	1.5	2.55242	−2.59602	1.66850	0.455149

Abbreviations: GM, gain margin; PM, phase margin.

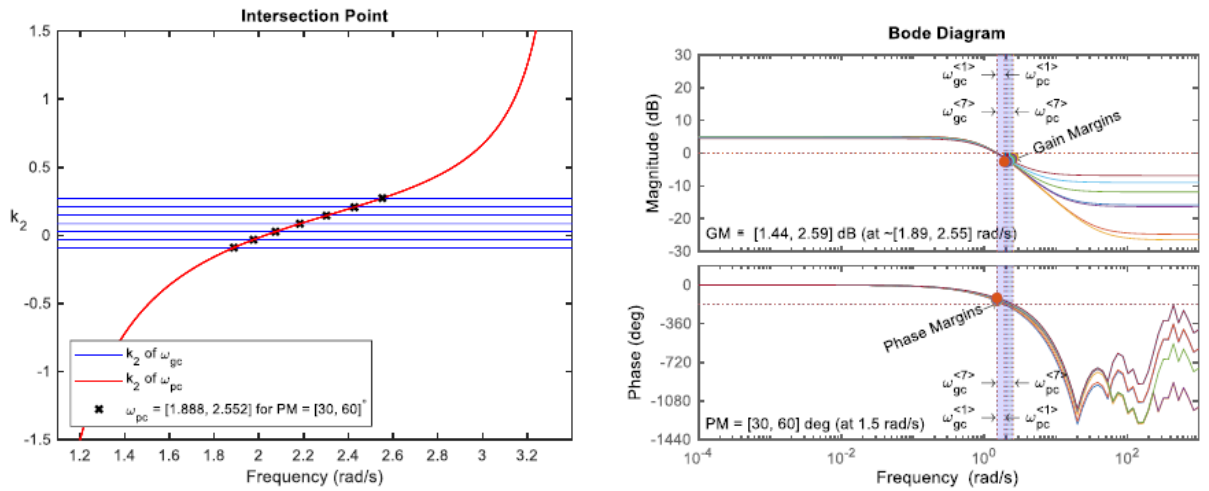

FIGURE 7 The intersection points of the k_2 values and Bode diagrams with $PM = [30°, 60°]$. [Colour figure can be **viewed at wileyonlinelibrary.com**]

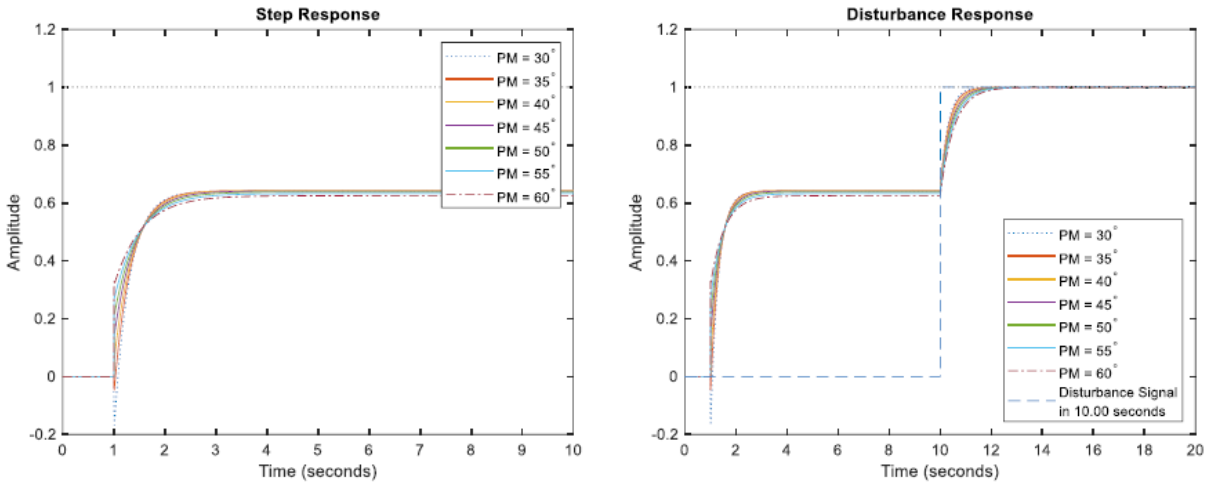

FIGURE 8 The step responses of all system and load disturbance reactions. [Colour figure can be **viewed atwileyonlinelibrary.com**]

10.2 Example 2: IOP with integrator

Consider Equation (**57**) as the plant in Example 1 with integrator to easily compare the results.

$$P_2(s) = \frac{1}{s}P_1(s) = \frac{1}{s(s+1)}e^{-s} \tag{57}$$

The desired gain crossover frequency for this example is $\omega_{gc} = 0.75$rad/s. **Table 2** shows the ω_{pc}, GM, k_p, and k_d values for PM values varying between 30° and 60°.

Again, in this condition, the change in the PM value shows its effect on the ω_{pc} as can be seen in **Table 2**. Similar to the previous example, **Figure 9** shows the intersection points and Bode diagrams of the system obtained with the PM in the range $PM = [30°, 60°]$.

The unit step responses and the step responses under load disturbance are given in **Figure 10**. It can be seen in the figure that the load disturbance yielded about 50% change in the peak point of the step response and the steady-state error is considerably reduced with the help of the integrator. As the result for this example, the desired frequency specifications are successfully met and the system achieved stability and improved robustness with the proposed method.

TABLE 2 For PM variations, k_p, k_d, ω_{pc}, and GM values were discovered.

PM	ω_{gc}	ω_{pc}	GM	k_p	k_d
30°	0.75	1.21752	−5.46910	0.88184	0.424279
35°	0.75	1.33211	−6.08356	0.85076	0.525141
40°	0.75	1.44064	−6.39401	0.81319	0.622007
45°	0.75	1.53620	−6.45022	0.76944	0.714139
50°	0.75	1.61731	−6.34206	0.71983	0.800836
55°	0.75	1.68555	−6.14820	0.66474	0.881439
60°	0.75	1.74336	−5.92236	0.60460	0.955332

Abbreviations: GM, gain margin; PM, phase margin.

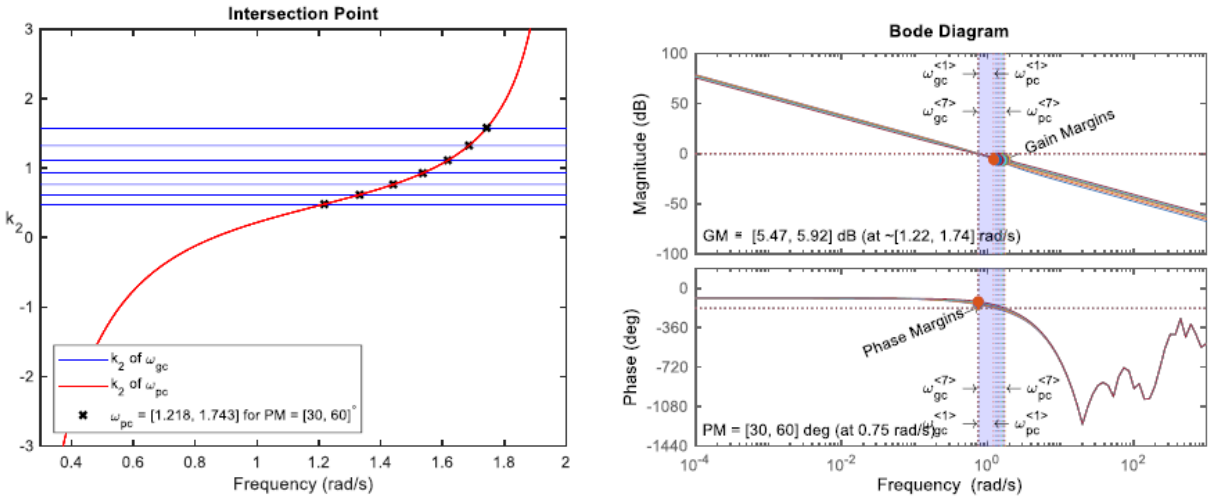

FIGURE 9 The intersection points to find the controller parameters and the Bode diagrams. [Colour figure can be **viewed at wileyonlinelibrary.com**]

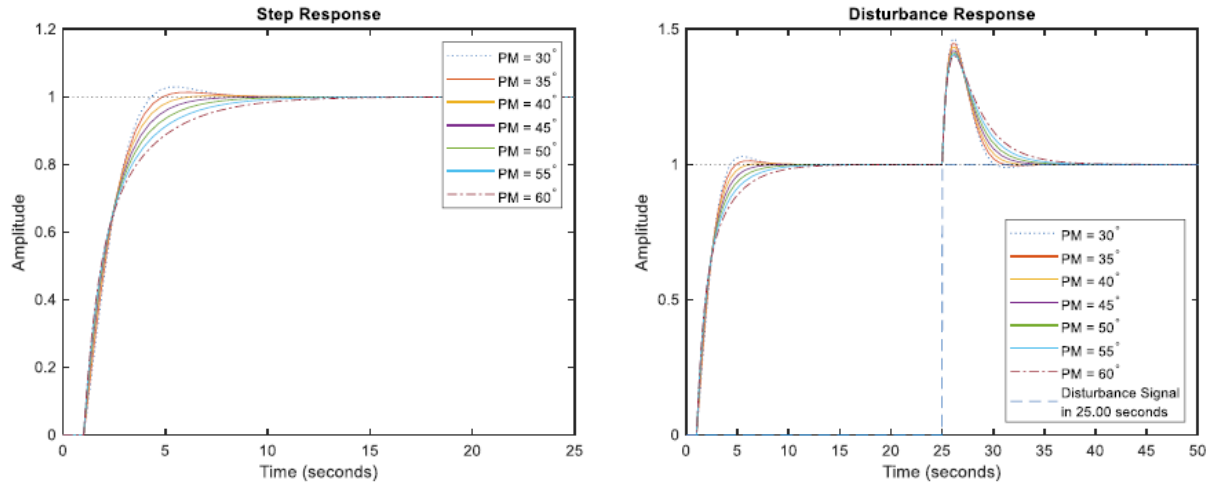

FIGURE 10 The step responses of all systems and load disturbance reactions. [Colour figure can be **viewed atwileyonlinelibrary.com**]

10.3 Example 3: Fractional order plant (FOP) with integrator

Let us reorganize the plant from Example 2 to Equation (**58**) by reducing the denominator order by 50%. Thus, an FOP is obtained.

$$P_2(s) = \frac{1}{s(s^{0.5}+1)} e^{-s} \tag{58}$$

In this case, $\omega_{gc} = 0.75$ rad/s is the desired gain crossover frequency. Similar to the previous example, **Table 3** shows the parameters of the system for PM values between 30° and 60°.

With the increase in PM, the ®pc also increases. Considering the fractional order version of the plant in the previous example, the value of ω_{pc} increased by around 25%. It can also be said that the fractional order affected the mpc value when compared to the IOP in Example 1.

Figure 11 shows the intersection points used to find the controller parameters as well as the Bode diagrams of the systems obtained for the changing PM values. Again, $\omega_{gc}^{<1>}$ stands for the gain crossover frequency of the system of $PM = 30°$ and $\omega_{gc}^{<7>}$ shows the gain crossover frequency to the system with $PM = 60°$.

Figure 12 shows the step responses without and with the load disturbance for the related systems. As a result of the unexpected load disturbance, the system exhibited a change of less than 40%.

TABLE 3 ω_{pc}, GM, k_p, and k_d values found for varying values of PM.

PM	ω_{gc}	ω_{pc}	GM	k_p	k_d
30°	0.75	1.26442	−5.62758	1.29076	0.113357
35°	0.75	1.42683	−6.73997	1.27844	0.262922
40°	0.75	1.61408	−7.55555	1.25639	0.410486
45°	0.75	1.80241	−7.85877	1.22478	0.554926
50°	0.75	1.96577	−7.67161	1.18384	0.695142
55°	0.75	2.09561	−7.19188	1.13390	0.830069
60°	0.75	2.19647	−6.59667	1.07532	0.958678

Abbreviations: GM, gain margin; PM, phase margin.

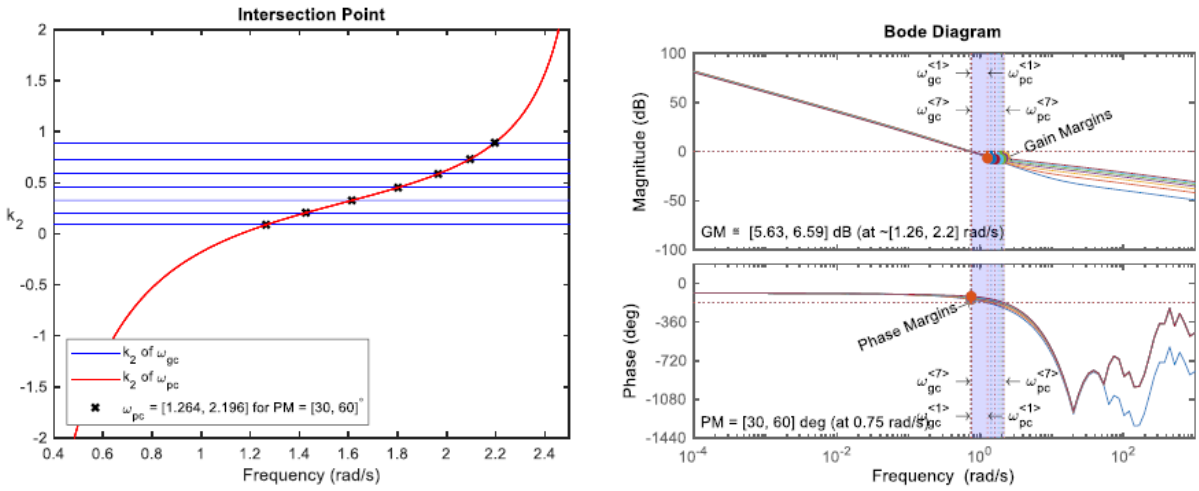

FIGURE 11 The intersection points to find the controller parameters and the Bode diagrams. [Colour figure can be viewed at **wileyonlinelibrary.com**]

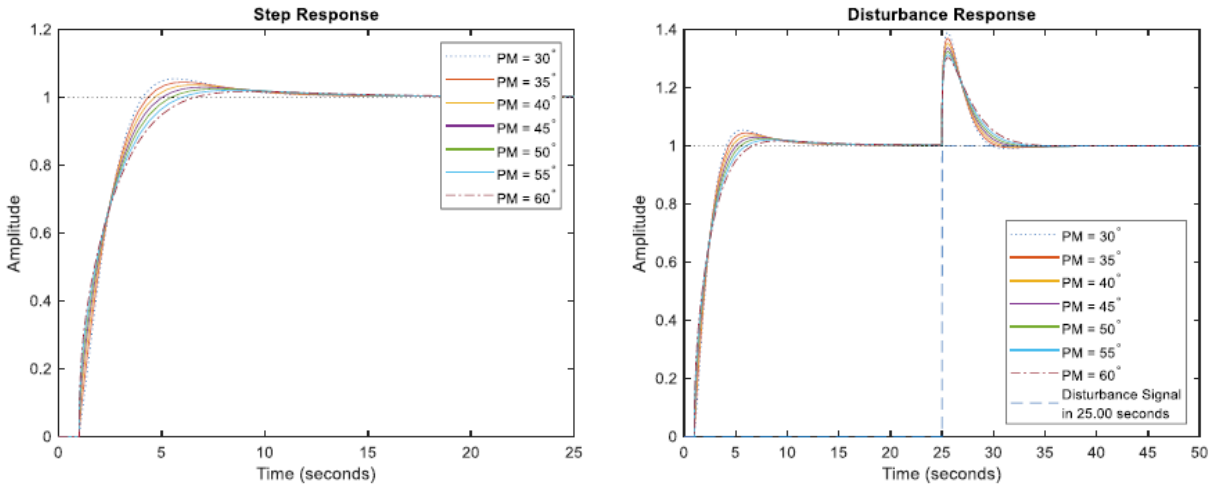

FIGURE 12 The system's step responses and load disturbance reactions. [Colour figure can be viewed at **wileyonlinelibrary.com**]

TABLE 4 ω_{pc}, GM, k_p, and k_d values found varying values of PM (negative complex part).

PM	ω_{gc}	ω_{pc}	GM	k_p	k_d
30°	0.75	1.93762	−9.90469	1.86650	0.829332
35°	0.75	2.15923	−9.86495	1.80519	1.043080
40°	0.75	2.32288	−9.40126	1.73014	1.248890
45°	0.75	2.44356	−8.78957	1.64192	1.445190
50°	0.75	2.53522	−8.16046	1.54120	1.630490
55°	0.75	2.60733	−7.56879	1.42876	1.803390
60°	0.75	2.66597	−7.03620	1.30544	1.962560

Abbreviations: GM, gain margin; PM, phase margin.

The proposed method successfully achieved the desired specifications and the system stability and robustness with the fractional order modified plant.

10.4 Example 4: Fractional complex order plant (FCOP) with integrator

We can add a complex coefficient to the denomintor order of the plant in Example 3 as given in Equation (**59**). The complex coefficient is given in its conjugate form.

$$P_{4,5}(s) = \frac{1}{s(s^{0.5 \mp j0.5} + 1)} e^{-s} \tag{59}$$

Let us determine the desired gain crossover frequency as $\omega_{gc} = 0.75$rad/s. **Table 4** shows the ω_{pc}, GM, k_p, and k_d found for PM values between 30° and 60° for the system with negative complex part of the complex order.

Table 4 shows that, in this case, the ω_{pc} value almost expanded with the same rate when compared to the plant in Example 3. We see that the system having negative conjugate of the complex order is exactly proportional to the system having fractional order on ω_{pc}.

Table 5 shows that the ω_{pc} value almost narrowed with the same rate when compared to the plant in Example 3. These results show that, when comparing with the FOP, the complex order plant has a direct effect on ω_{pc} and inversely proportional to the positive complex component.

TABLE 5 ω_{pc}, GM, k_p, and k_d values found varying values of PM (positive complex part).

PM	ω_{gc}	ω_{pc}	GM	k_p	k_d
30°	0.75	1.12531	−3.65564	0.99588	−0.159541
35°	0.75	1.22879	−4.52686	1.00251	−0.043206
40°	0.75	1.35516	−5.39434	1.00152	0.073458
45°	0.75	1.50702	−6.12772	0.99291	0.189563
50°	0.75	1.67726	−6.53189	0.97674	0.304226
55°	0.75	1.84546	−6.47330	0.95314	0.416573
60°	0.75	1.99117	−6.01925	0.92228	0.525750

Abbreviations: GM, gain margin; PM, phase margin.

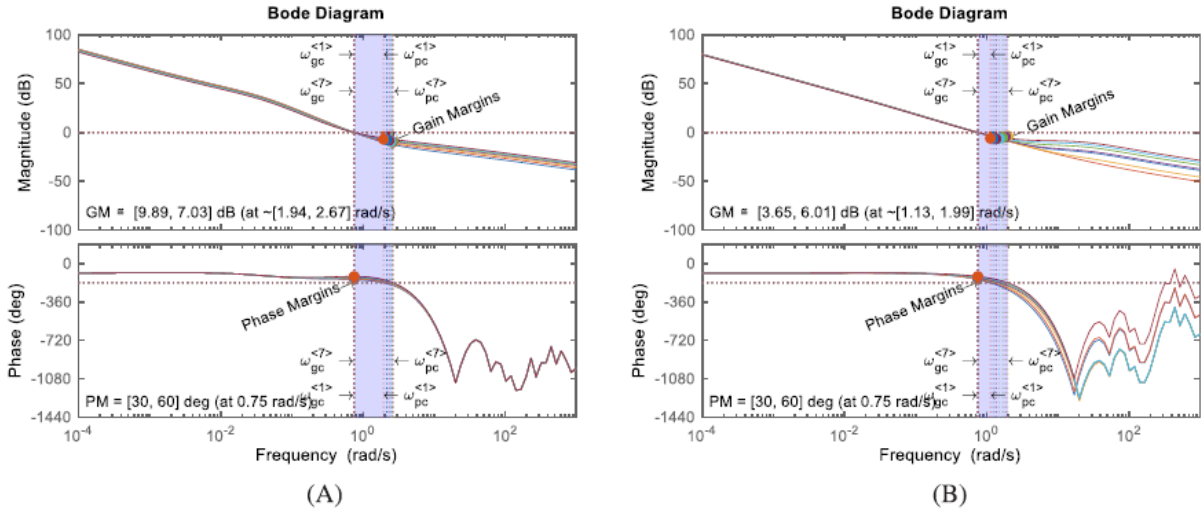

(A) (B)

FIGURE 13 The Bode diagrams. (A) shows the Bode diagram of the systems having the negative complex part, and (B) gives the Bode diagram with the positive complex part. [Colour figure can be viewed at **wileyonlinelibrary.com**]

Figure 13A shows the Bode diagram of the systems having the negative complex part, and **Figure 13B** gives the Bode diagram with the positive complex part.

Similarly, **Figure 14A** shows the intersection points for the system with the negative complex part and **Figure 14B** gives the intersection points for the system with the positive complex part.

11 DISCUSSIONS

In this study, a plant model representing all the possibilities including integer, fractional and complex coefficients, and orders that can have time delay and extra gain coefficient is proposed. A classical PD

controller is assumed to control the mentioned plant. The design approach is even more important when it comes to minimizing system failures due to unexpected load disturbance signals that a system may encounter. At the same time, it has become vital to test and discuss the findings in a simulation environment in order to reduce the costs arising from these errors.

The IOP is described initially in this research. Due to the lack of an integrator in the $IOPD$ controller structure, an integrator component was added to the controller in order to reduce the steady-state error. The FOP is studied in order to reduce the overshoot time in response to unanticipated load disturbance signals of the system by altering the denominator order by 50%. Finally, by adding a complex component to this fractional value, the $FCOP$ is explained.

Figure **15A,B** shows step response and load disturbance response for a system with a PM of 45°, respectively.

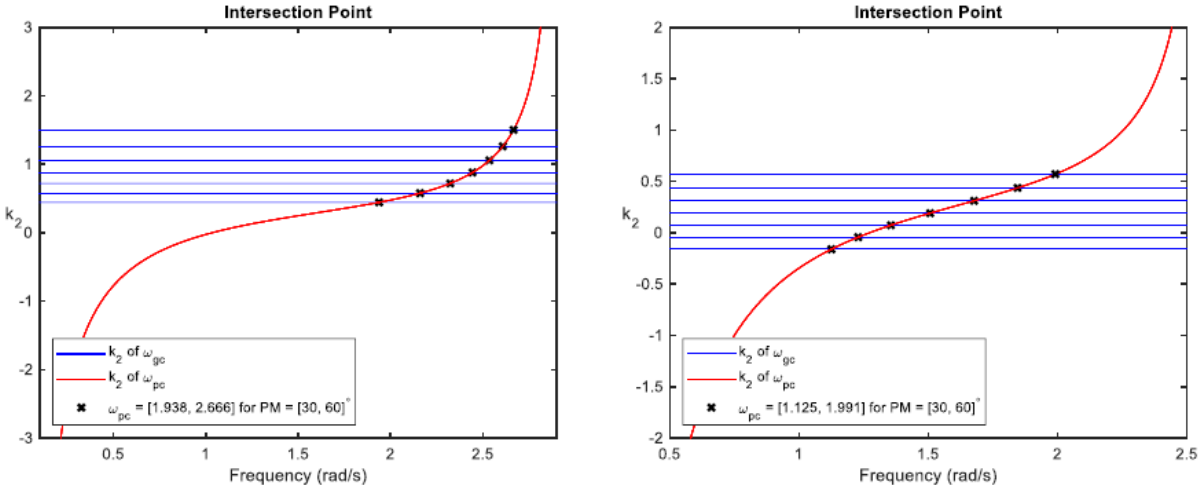

(A) (B)

FIGURE 14 The intersection points. (A) shows the intersection points for the system with the negative complex part, and (B) gives the intersection points for the system with the positive complex part. [Colour figure can be viewed at **wileyonlinelibrary.com**]

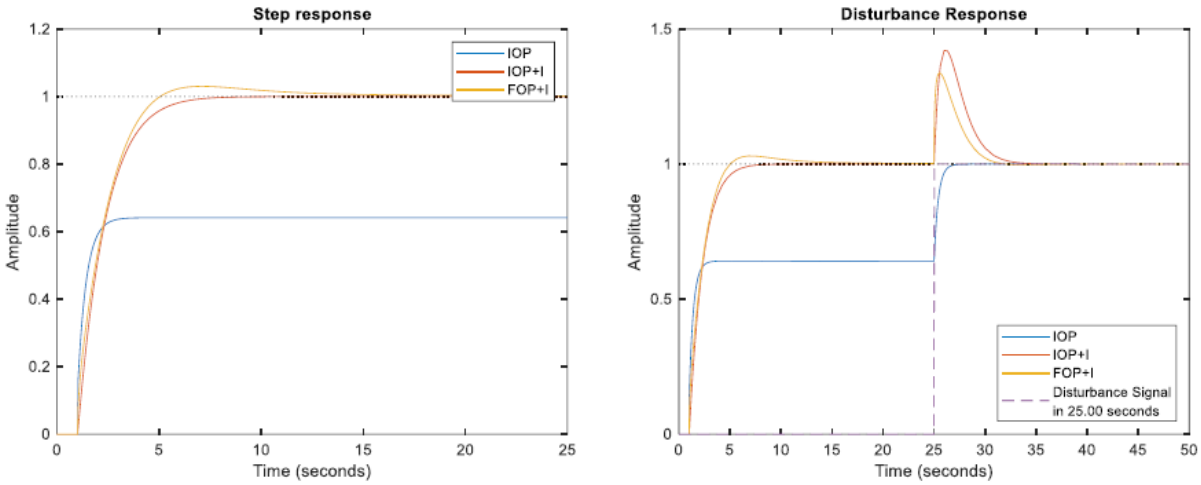

(A) (B)

FIGURE 15 The systems' step response and load disturbance reaction with $PM = 45°$. (A) shows step response and (B) load disturbance response for a system with a PM of 45°. [Colour figure can be viewed at **wileyonlinelibrary.com**]

It is clear in **Figure 15** that the IOP has a greater steady-state intolerance if the controller did not include an integrator. The plant with the $IOP + I$ (integrator) seemed to have the lowest steady-state error. With the $FOP + I$, the settling time and overshoot time were enhanced even more. As a consequence, comparing the plants with and without integrator resulted that the $FOP + I$ demonstrated reduced system error and quicker system stability response under unexpected load disturbance signal.

Let us study all the examples illustratively. The desired ω_{gc} for the first example is $\omega_{gc} = 1.5$ rad/s and for the remaining are $\omega_{gc} = 0.75$rad/s. The PM is selected to be 45°. Bode diagrams of the systems in the examples are shown in **Figure 16A,B** as a general view and a closer view, respectively.

In the figure, $i \rightarrow$ corresponds to the ω_{gc} and $\leftarrow i$ shows the ω_{pc} of the ith case (the cases are IOP, $IOP + 1, FOP + 1, FCOP + I - j, FCOP + 1 + j$, respectively). It can be seen in the figure that the ®pc value is directly affected although the PM was not changed. The ®pc value of the system having negative complex conjugate is calculated to be smaller than the one having positive complex part.

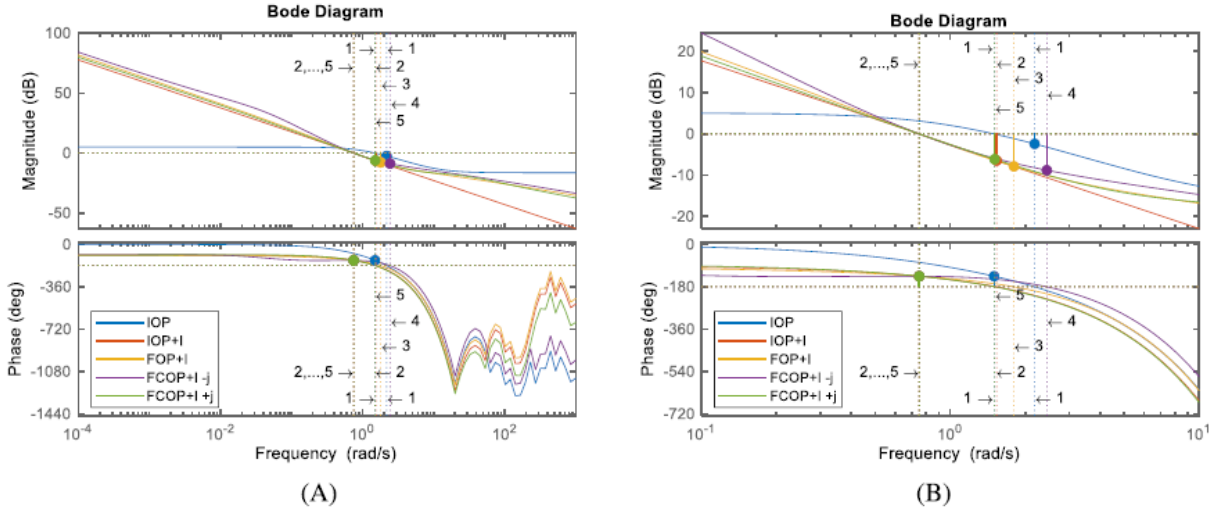

FIGURE 16 The Bode diagrams with $PM = 45°$. Bode diagrams of the systems in the examples are shown in as (A) a general view and (B) a closer view. [Colour figure can be viewed at **wileyonlinelibrary.com**]

Starting from an IOP and modifying the plant as the other forms, the Bode diagram gives clues about the changes in the behavior of the system with the changing value of the ω_{pc}. It is seen that, when compared with the $IOP + 1$ system, the ω_{pc} of the $FOP + 1$ system is reduced, but the ω_{pc} is increased with the $FCOP + I - j$ case. The fact that the complex part does not cause a visible change in the GM of the system but yields to a significant variation in the PM further supports the complex number theory. The positive and negative values of the complex component are not limited to determining the position of the phase transition frequency only. It also shows that by increasing the negative values of the complex component, the phase curve of the system will be pulled up from the instability line and will increase the robustness of the system. Taking larger values causes the phase curve of the system to fall further below the instability line.

12 CONCLUSION

On the contrary to similar researches, the plant model with the most broad structure is used in this study, which focuses on the most realistic investigation of physical changes. The most significant

contribution to the literature of this study is the contribution of complex plant models to system stability and robustness, as well as associated physical phenomena. It is preferred to use the classical proportional derivative controller to control IOP, FOP, and $FCOP$ models in order to achieve this goal. Analyses of the above plants and their modifications having an integrator have been revealed the differences and advantages of the controller consisting of the proportional and derivative operators. Bode diagram restrictions are also used to develop the equations for the system stability and robustness. Simultaneously, the system's response to unexpected load disturbances was explored. Finally, the findings and visuals were acquired under the same conditions in each of the four application cases presented, and the superiority of the systems to each other and their physical interpretations were addressed. Despite the fact that many studies in the literature include both integer and FOPs, we believe that this study covers all system types. The determinations and discussions, as well as the calculation formulae that are easily produced in this challenging field of study, can be considered of a quality that can be innovative. Different physical behaviors are predicted to arise and be interpreted in future investigations as the obtained parameters are changed.

REFERENCES

1. Y. Li, K. H. Ang, and G. C. Chong, PID control system analysis and design, IEEE Control Syst Mag **26** (2006), no. 1, 32-41.
2. J. G. Ziegler and N. B. Nichols, Optimum settings for automatic controllers, Trans ASME **64** (1942), no. 8, 759-765.
3. N. Tan, Computation of stabilizing PI-PD controllers, Int J Control Autom Syst **7** (2009), no. 2, 175-184.
4. K. J. Åström and T. Hagglund, The future of PID control, Control Eng Pract **9** (2001), no. 11, 1163-1175.
5. K. Ranjbaran and M. Tabatabaei, Fractional order [PI],[PD] and [PI][PD] controller design using Bode's integrals, Int J Dyn Control **6** (2018), no. 1, 200-212.
6. I. Podlubny, Fractional differential equations, Academic Press, San Diego, CA, 1999.
7 .D. Valério and J. S. Da Costa, Introduction to single-input, single-output fractional control, IET Control Theory Appl **5** (2011), no. 8,1033-1057.
8. A. Guefrachi, S. Najar, M. Amairi, and M. Aoun, Tuning of fractional complex order PID controller, IFAC-PapersOnLine **50** (2017), no. 1, 14563-14568.
9. J. Sabatier, P. Lanusse, P. Melchior, and A. Oustaloup, Fractional order differentiation and robust control design, Intell Syst Control Autom: Sci Eng **77** (2015), 13-18.
10. J. Liouville, Sur le calcul des differentielles indices quelconques, J Ec Polytech - Math **71** (1832), 240-252.
11. B.Riemann, Gesammelte mathematische Werke und wissenschaftlicher Nachlass, Vol. **1**, BG Teubner, 1876.
12. O. W. Abdulwahhab, Design of a complex fractional order PID controller for a first order plus time delay system, ISA Trans **99** (2020), 154-158.

13. K. Bingi, R. R. Kulkarni, and R. Mantri, Design and Analysis of Complex Fractional-order PID Controllers, In 2021 IEEE Madras section conference (MASCON), 2021.

14. M. Zheng, T. Huang, G. Zhang, and D. Zhong, Stability region Design of Fractional Complex Order $ $PI^{\lambda+\mu\mathrm {i}} $ controller using D segmentation, 2019 6th international conference on systems and informatics (ICSAI), 2019.

15. P. Sathishkumar and N. Selvaganesan, Tuning of complex coefficient PI/PD/PID controllers for a universal plant structure, Int J Control **94** (2021), no. 11, 3190-3212.

16. P. Sathishkumar and N. Selvaganesan, Fractional controller tuning expressions for a universal plant structure, IEEE Contr Syst Lett **2** (2018), no. 3, 345-350.

17. O. Hanif, G. B. Babu, and S. Sharma, Performance improvement of PI x+ iy D fractional complex order controller using genetic algorithm, 2018 fourth international conference on advances in electrical, Electronics, Information, Communication and Bio-Informatics (AEEICB), 2018.

18. R. Sekhar, T. P. Singh, and P. Shah, Complex order PI a D y design for surface roughness control in machining CNT Al-mg hybrid composites, Adv Sci Technol Eng Syst **J 5** (2020), 299-306.

19. N. Saikumar, D. Valério, and S. H. HosseinNia, Complex order control for improved loop-shaping in precision positioning, In 2019 IEEE 58th conference on decision and control (CDC), 2019.

20. G. Wang, K. Yang, H. Gu, F. Guan, and A. H. Kara, A (2+ 1)-dimensional sine-Gordon and sinh-Gordon equations with symmetries and kink wave solutions, Nucl Phys B **953** (2020), 114956.

21. G. Wang, A novel (3+1)-dimensional sine-Gorden and a sinh-Gorden equation: derivation, symmetries and conservation laws, Appl Math Lett **113** (2021), 106768.

22. G. Wang, A new (3+1)-dimensional Schrodinger equation: derivation, soliton solutions and conservation laws, Nonlinear Dyn **104** (2021), no. 2, 1595-1602.

23. G.Wang, Symmetry analysis, analytical solutions and conservation laws of a generalized KdV-burgers-Kuramoto equation and its fractional version, Fractals **29** (2021), no. 4, 2150101.

24. G. Wang and A. M. Wazwaz, A new (3+ 1)-dimensional KdV equation and mKdV equation with their corresponding fractional forms, Fractals **30** (2022), no. 4, 1-8.

25. G. Wang and A. M. Wazwaz, On the modified Gardner type equation and its time fractional form, Chaos Solit Fractals **155** (2022), 111694.

26. D. Valério, N. Saikumar, A. A. Dastjerdi, N. Karbasizadeh, and S. H. HosseinNia, Reset control approximates complex order transfer functions, Nonlinear Dyn **97** (2019), no. 4, 2323-2337.

27. M. Shahiri, A. Ranjbar, M. R. Karami, and R. Ghaderi, New tuning design schemes of fractional complex-order PI controller, Nonlinear Dyn **84** (2016), no. 3, 1813-1835.

28. K. Khandani, A. A. Jalali, and M. R. R. Mehdiabadi, Robust complex order controller design for DC motors, 20th Iranian conference on electrical engineering (ICEE2012), 2012.

29. N. Karbasizadeh and S. H. HosseinNia, Complex-order reset control system, 2022IEEE/ASME International Conference on Advanced Intelligent Mechatronics (AIM), (2022).

30. A. V. Tare, J. A. Jacob, V. A. Vyawahare, and V. N. Pande, Design of novel optimal complex-order controllers for systems with fractional-order dynamics, Int J Dyn Control **7** (2019), no. 1, 355-367.

31. M. Zheng, G. Zhang, and T. Huang, Tuning of fractional complex-order direct current motor controller using frequency domain analysis, Math Methods Appl Sci **44** (2021), no. 4, 3167-3181.

32. J. L. Adams, T. T. Hartley, and L. I. Adams, A solution to the fundamental linear complex-order differential equation, Adv Eng Softw **41** (2010), no. 1, 70-74.

33. J. L. Adams, R. J. Veillette, and T. T. Hartley, Conditions for stable and causal conjugate-order systems, In 2010 IEEE international symposium on industrial electronics, 2010.

34. J. A. Jacob, A. V. Tare, V. A. Vyawahare, and V. N. Pande, A review of time domain, frequency domain and stability analysis of linear complex-order systems, 2016 IEEE international WIE conference on electrical and computer engineering (WIECON-ECE), 2016.

35. M. F. Silva, J. T. Machado, and R. S. Barbosa, Complex-order dynamics in hexapod locomotion, Signal Process **86** (2006), no. 10, 2785-2793.

36. C. Pinto and J. T. Machado, Complex order van der Pol oscillator, Nonlinear Dyn **65** (2011), no. 3, 247-254.

37. B.Şenol, U. Demiroğlu, and R. Matušů, Fractional order proportional derivative control for time delay plant of the second order: the frequency frame, J Franklin Inst Eng Appl Math **357** (2020), no. 12, 7944-7961.

38. B. Şenol and U. Demiroğlu, Fractional order proportional derivative control for first order plus time delay plants: achieving phase and gain specifications simultaneously, Trans Inst Meas Control **41** (2019), no. 15, 4358-4369.

39. C. Wang, Y. Jin, and Y. Q. Chen, Auto-tuning ofFOPI and FO [PI] controllers with iso-damping property, In Proceedings of the 48h IEEE conference on decision and control (CDC) held jointly with 2009 28th Chinese control conference, 2009.

40. V. Pommier-Budinger, Y. Janat, D. Nelson-Gruel, P. Lanusse, and A. Oustaloup, Fractional robust control with iso-damping property, In 2008 American control conference, 2008.

41. Y. Q. Chen, K. L. Moore, B. M. Viangre, and I. Podlubny, Robust PID controller autotuning with an Iso-damping property through a phase shaper, Fract Differ Appl (2005), 687-706.

42. J. Edmunds, Control system design and analysis using closed-loop Nyquist and Bode arrays, Int J Control **30** (1979), no. 5, 773-802.

43. A. C. Bartlett, Nyquist, Bode, and Nichols plots of uncertain systems, In 1990 American control conference, 1990.

44. K. J. Åström, T. Hägglund, and K. J. Astrom, Advanced PID control, ISA-The Instrumentation, Systems, and Automation Society, Research Triangle Park, 2006.

45. Y. Zhang, C. M. Akujuobi, W. H. Ali, C. L. Tolliver, and L. S. Shieh, Load disturbance resistance speed controller design for PMSM, IEEE Trans Ind Electron **53** (2006), no. 4, 1198-1208.

46. S. Tufenkci, B. Senol, B. B. Alagoz, and R. Matušů, Disturbance rejection FOPID controller design in v-domain, J Adv Res **25** (2020), 171-180.

47. C. Onat, S. E. Hamamci, and S. Obuz, A practical PI tuning approach for time delay systems, IFAC Proc **45** (2012), no. 14, 102-107.